Powder-metallurgical processing and phase separation in ternary transition metal carbides

Taoran Ma

Doctoral Thesis 2017

Unit of Structures

Department of Materials Science and Engineering

School of Industrial Engineering and Management

KTH Royal Institute of Technology

Stockholm, Sweden

Powder-metallurgical processing and phase separation in ternary transition metal carbides

Unit of Structures

Department of Materials Science and Engineering

School of Industrial Engineering and Management

KTH Royal Institute of Technology

SE-100 44 Stockholm, Sweden

ISBN: 978-91-7729-439-9

Akademisk avhandling som med tillstånd av Kungliga Tekniska Högskolan i Stockholm framlägges till offentlig granskning för avläggande av Teknologie Doktorsexamen torsdag den 15 juni 2017 kl 10:00 i sal B2, Brinellvägen 23, Kungliga Tekniska Högskolan, Stockholm.

The PDF version of this thesis is available at kth.diva-portal.org

Printed by Universitetsservice US-AB, Stockholm, Sweden

Abstract

Ternary transition metal cubic carbides have high hardness and are potential carbides in cemented carbide and cermet tools, as well as hard coatings used to improve metal cutting performance. In the present work, (Ti,Zr)C, (V,Nb)C, and (V,Ta)C ternary cubic carbides were synthesized using traditional powder-metallurgical methods. The effect of synthesis temperature and starting materials on synthesis is investigated, and the microstructure evolution during aging is studied.

(Ti,Zr)C was found to decompose into lamellae upon aging at the temperature range from 1150 to 1800 °C. A similar microstructure was observed in (V,Ta)C and (V,Nb)C- 0.5 wt% Fe. All of these structures were found to form through discontinuous precipitation.

The grain misorientation distribution of (Ti,Zr)C aged at 1400 °C is investigated. It was found that decomposition tends to occur at high-angle grain boundaries above 25°.

The hardness of as-synthesized (Ti,Zr)C powder was found to be 41 ± 6 GPa. Fully decomposed (Ti,Zr)C particles were found to be slightly softer, with a hardness of 34 ± 3 GPa. On the other hand, in (V,Nb)C-0.5 wt% Fe, the decomposed structure formed upon aging at 1200 °C was found to have a hardness of 26 ± 2 GPa, which is basically the same as the unaged alloy.

Furthermore, the sintering behavior of (Ti,Zr)C with WC-Co is investigated. There are two γ-phases in the final microstructure, one TiC-rich and one ZrC-rich. (Ti,Zr)C was found to decompose at an early stage of sintering, and

the final grain size of WC and the two γ-phases was found to be 10% smaller than that in a reference WC-TiC-ZrC-Co composite.

Sammanfattning

Ternärna kubiska karbider av övergångsmetaller har hög hårdhet och kan potentiellt användas i verktyg för skärande bearbetning såsom hårdmetall, cermets eller som tunna nötningsbeständiga skikt. I det nuvarande arbetet har de kubiska karbiderna (Ti,Zr)C, (V,Nb)C och (V,Ta)C syntetiserats med användning av traditionella pulvermetallurgiska metoder. Effekten av syntestemperatur och utgångsmaterial på syntesen har undersökts, och mikrostrukturens utveckling under åldrandet har också studerats.

(Ti,Zr)C sönderfaller i lameller, med början vid korngränserna eller pulverpartiklarnas ytterytor, vid åldring i temperaturområdet 1150 till 1800 °C. Liknande mikrostrukturer observeras i (V,Ta)C och (V,Nb)C-0,5 vikt% Fe efter åldring. Mekanismen för sönderfallet visar sig vara diskontinuerlig utskiljning.

Inverkan av korngränsernas orientering på det diskontinuerliga sönderfallet hos (Ti,Zr)C efter åldring vid 1400 °C har undersökts. Sönderfallet tenderar att uppträda vid högvinkliga korngränser över 25 °.

Hårdheten hos syntetiserat (Ti,Zr)C pulver är 41±6 GPa. De fullständigt sönderfallna (Ti,Zr)C partiklarna är något mjukare, med en hårdhet av 34±3 GPa. Å andra sidan, i (V,Nb)C-0,5 vikt% Fe uppvisar den sönderfallna strukturen, som bildas vid åldring vid 1200 °C, en hårdhet av 26±2 GPa, som är ungefär samma som för den oåldrade legeringen.

Vidare undersöktes sintringsbeteendet hos (Ti,Zr)C med WC-Co. Det finns två γ-faser i den sintrade mikrostrukturen: en TiC-rik och en ZrC-rik.

(Ti,Zr)C sönderfaller i ett tidigt skede under sintringen och den slutliga kornstorleken hos WC och de två γ-faserna var 10 % mindre jämfört med en referenslegering WC-TiC-ZrC-Co.

Appended papers

I. Microstructure evolution during phase separation in Ti-Zr-C
Taoran Ma, Rafael Borrajo-Pelaez, Peter Hedström, Ida Borgh, Andreas Blomqvist, Susanne Norgren, Joakim Odqvist

International Journal of Refractory Metals and Hard Materials 2016; 61: 238-248

II. Synthesis, aging and nano-hardness of Ti-Zr-C
Taoran Ma, Peter Hedström, and Joakim Odqvist

In manuscript.

III. Self-organizing nanostructured lamellar (Ti,Zr)C – A superhard mixed carbide
Taoran Ma, Peter Hedström, Valter Ström, Ansar Masood, Ida Borgh, Andreas Blomqvist, Joakim Odqvist

International Journal of Refractory Metals and Hard Materials 2015; 51: 25-28

IV. Powder-metallurgical synthesis and aging of (V,Nb)C and (V,Ta)C
Taoran Ma, Peter Hedström, and Joakim Odqvist,

In manuscript

V. Liquid phase sintering of (Ti,Zr)C with WC-Co
Taoran Ma, Rafael Borrajo-Pelaez, Peter Hedström, Andreas Blomqvist, Ida Borgh, Susanne Norgren, and Joakim Odqvist

Materials 2017; 10: 57

My contribution to the appended papers

I. I took part in the planning of the work, performed a major part of the experiments and analysis, and drafted the manuscript.

II. I took part in the planning of the work, performed a major part of the experiments and analysis, and drafted the manuscript.

III. I took part in the planning of the work, performed a large part of the experiments and major part of analysis, and drafted the manuscript.

IV. I took part in the planning of the work, performed a major part of the experiments and analysis, and drafted the manuscript.

V. I took part in the planning of the work, performed a large part of the experiments and a major part of analysis and calculation, and drafted the manuscript.

Contents

Chapter 1

Introduction

Cemented carbides and cermets are widely used in cutting tools for metal machining. Both are bulk composites that consist of hard grains of carbides or carbonitrides embedded in a tough binder of Co or Ni-Co alloy. Their cutting performance can be further enhanced by hard coatings, which usually consist of nitrides or carbonitrides [1].

Transition metal cubic carbides and carbonitrides, particularly those from IVB and VB groups, can be used as the second hard phase (γ-phase) in cemented carbides, as hard phase in cermets, and in wear-resistant coatings [2,3].

It has been found that ternary carbides, nitrides, and carbonitrides may perform better than their binary counterparts. For instance, Pandemo [4] found that (Ti,Hf)C and (V,Nb)C exhibit higher hardness than their binary counterparts. Holleck [5] proposed that this is due to hardening via phase separation.

A few ternary carbide systems contain miscibility gaps, e.g., (Ti,Hf)C, (Ti,Zr)C, (V,Nb)C, and (V,Ta)C [6]. Phase separation occurs within a miscibility gap and could possibly be utilized as a hardening mechanism. Phase separation is a way to tune the mechanical properties. A reported

example is TiAlN, which decomposes into TiN and AlN nano-structures, resulting in high hardness [7–9]. It is important to understand the phase stability of ternary carbides before they are used as constituents in hard metals. The present work aims to investigate the microstructure evolution during phase separation using experimental methods.

1.1 Scope of the work

This work aims to investigate the powder-metallurgical synthesis of (Ti,Zr)C, (V,Nb)C, and (V,Ta)C and their phase separation behavior. For (Ti,Zr)C, the synthesis was performed using $TiZrO_4$ powder and carbon black powder at different temperatures. As-synthesized (Ti,Zr)C was then aged to investigate the phase separation.

Similarly, (V,Nb)C and (V,Ta)C were investigated. They were synthesized from corresponding binary carbide powders, which were mixed using different methods—milling or mortar—to investigate the effect of mixing on synthesis. The effect of adding Fe was also investigated. Subsequently, the as-synthesized ternary carbides were aged at temperatures inside the miscibility gap.

The phases present before and after aging were investigated by X-ray diffraction (XRD). The morphology of as-synthesized samples and decomposition structures generated upon different aging conditions were investigated using scanning electron microscopy (SEM) and backscattered electron microscopy (BSE). To study the composition of different microstructure features, energy dispersive X-ray spectroscopy (EDS) was applied, and the measurements were performed at optimized accelerating voltages. The electron backscatter diffraction (EBSD) technique was used to investigate the orientation relation between decomposed structure and original matrix, based on which the mechanism of phase separation was thus studied. Moreover, the local hardness of different microstructure was determined using nano-indentation technique.

Besides the investigations of the ternary systems, the sintering behavior of (Ti,Zr)C with WC-Co, in comparison with those sintered from binary carbides, was also investigated. The different sintering stages with regard to shrinkage rate of the composites was determined by a dilatometer, and the melting behavior was monitored by differential scanning calorimetry (DSC). To study the microstructural evolution, a series of interrupted sintering trials were performed in DSC. The phases present at different sintering temperatures were then investigated by SEM-BSE, and composition was detected by EDS.

Chapter 2

Ternary transition metal carbides

Ternary transition metal cubic carbides are a solid solution consisting of two transition metals from the IVB and VB groups, i.e., Ti, Zr, Hf, V, Nb, and Ta, together with carbon. These cubic carbides have the NaCl type of crystal structure, in which metal atoms comprise a face-centered cubic (fcc) lattice, and carbon atoms fill the interstitial positions [10].

2.1 Preparation of ternary carbides

Ternary carbides can be produced through a variety of methods, such as carburization of metal mixtures, carbothermal reduction of oxides, and thermal synthesis of binary carbides [11].

Carburization of metal mixtures

An approach of using Ti, Zr, and carbon powder mixtures to prepare ternary (Ti,Zr)C carbides was reported by Teber et al. [12]. The mixtures were firstly ball milled, and nano-crystalline (Ti,Zr)C powders were produced through mechanical alloying. Afterwards, the nano-powders were sintered to $Ti_{0.8}Zr_{0.2}C$ bulk samples in a spark plasma sintering apparatus up to 1800 °C. Similarly, Liu et al. [13] synthesized a series of (Ti,Zr)C bulk pieces by sintering pellets made of Ti and Zr nano-powders in a graphite die in a spark plasma sintering system up to 2100 °C.

Carbothermal reduction of metal oxides

Oxide mixtures with sufficient carbon black powder can be used as starting materials to produce ternary carbide solid solutions. Lee and Ha [14] synthesized (Ti,W)C_x nano-powder by heating composite oxide powder—with a mixed phase structure of TiO_2 and WO_3—and carbon black at 1400 °C.

Borgh et al. [15] produced near-single phase (Ti,Zr)C powder with micro-sized particles through carburization of $TiZrO_4$ nano-powder with carbon black at 2200 °C. It was found that the carbide phase inside particles is $Ti_{0.35}Zr_{0.65}C$, while the carbide phase in the particle surface contain much higher content of Ti (see further details in Paper I). A concentration gradient with an average composition of $Ti_{0.49}Zr_{0.51}C$ was observed in the vicinity of particle surfaces.

Using the same procedure as in [15], (Ti,Zr)C powder was synthesized at 2200 °C, 2300 °C, and 2400 °C in the work described in Paper II. It was found that the synthesis temperature affects porosity (Figure 1) and composition homogeneity (Figure 2 and Paper II). As the temperature increases, both structural and compositional homogeneity improve.

Synthesis from binary carbides

Ternary carbides can be formed by heating corresponding binary carbide powders to high temperatures where the solid solution is thermodynamically stable. Li et al. [16] synthesized (Ti,Zr)C bulk samples using TiC and ZrC powders in spark plasma sintering equipment up to 2200 °C.

To produce very pure solid solutions in a short time, diffusion-promoting agents, e.g., cobalt, nickel, and so forth, in quantities of 0.5 % - 5 %, is recommended [11]. By adding 1 wt % of Co powder, Norton and Mowry [17] synthesized a series of (Zr,Ta)C, (Nb,Zr)C, (Nb,Ta)C, and (Ti,Zr)C in a high-frequency vacuum furnace at 2100 °C.

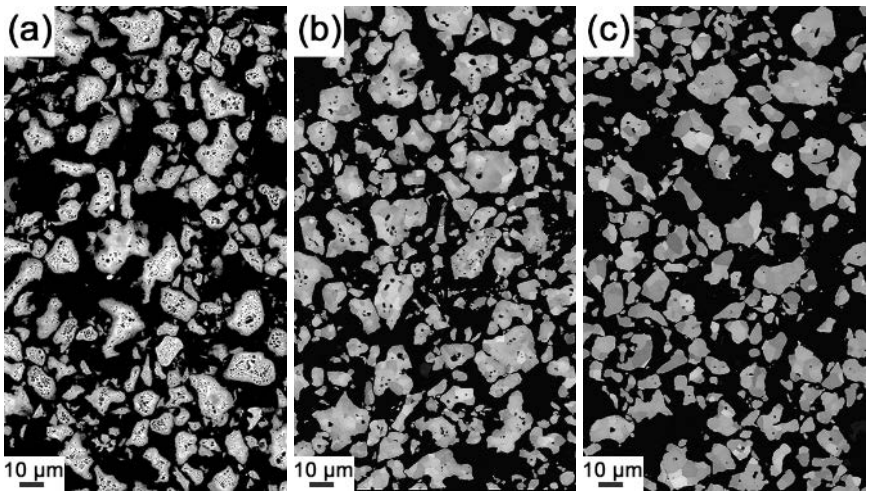

Figure 1. (Ti,Zr)C particles synthesized at (a) 2200 °C, (b) 2300 °C, and (c) 2400 °C. Porosity decreases with increasing synthesis temperature.

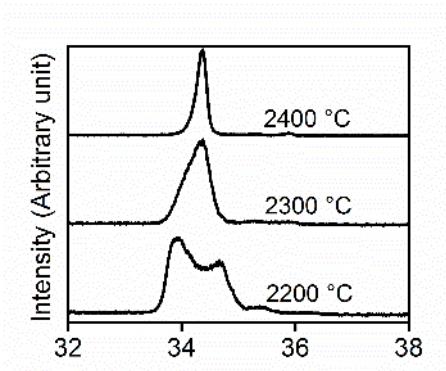

Figure 2. XRD diffraction patterns of (Ti,Zr)C synthesized at 2200 °C, 2300 °C, and 2400 °C.

In Paper IV, (V,Nb)C and (V,Ta)C bulk samples were synthesized from VC, NbC, or TaC powders in a graphite furnace at 2200 °C. Fe powder (0.5 wt %) was added to selected samples to act as a diffusion aid. It was found that the size of pores in as-synthesized ternary carbide decreases if the starting powders are ball milled (see Figure 3a and b). This is because milling can effectively

reduce the particle size of micron sized powder particles. Moreover, the porosity can be further reduced by the addition of Fe (see Figure 3).

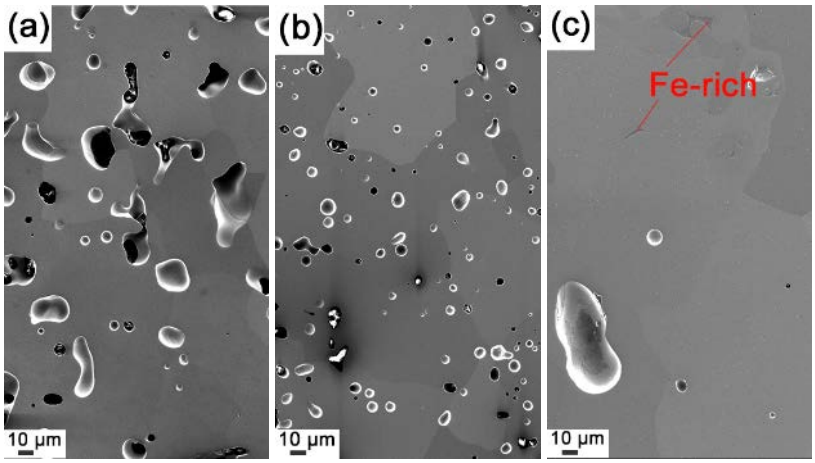

Figure 3. (V,Nb)C synthesized from binary carbide powders mixed in different conditions: (a) mortar, (b) milling, and (c) milling with the addition of Fe.

2.2 Miscibility

In some ternary carbide systems, e.g., (Ti,Zr)C, (Ti,Hf)C, (V,Nb)C, and (V,Ta)C, the ternary solid solution is stable at high temperatures but demixes to binary carbides at low temperatures due to the immiscibility between each other [5,6,18]. Both the ternary carbide solid solution and as-decomposed phases have the same crystal structure. Such a system contains a miscibility gap in the phase diagram (see Figure 4).

Inside the miscibility gap, there is a chemical spinodal region, within which the system is unstable; theoretically, the decomposition would occur without overcoming any energy barrier, except the activation energy for diffusion. Between the spinodal and miscibility gap, the system is metastable, and to decompose, the system must overcome a barrier, i.e., a nucleation event must first take place.

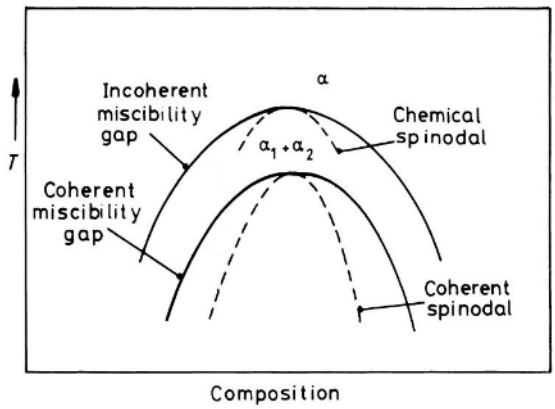

Figure 4. Schematic miscibility gap. Coherent miscibility gap is suppressed to lower temperatures when coherency strain exists [19].

In real systems, the atomic size of the end members is usually different. Considering a system with composition X_0 and corresponding lattice parameter a, any composition change ΔX would result in a change in lattice parameter. A fractional change in lattice parameter per unit composition change can be expressed as

$$\eta = \frac{1}{a}\left(\frac{da}{dX}\right)$$

The difference in the atomic size introduces coherency strain energy, ΔG_s, to the system.

$$\Delta G_s = \eta^2 (\Delta X)^2 E' V_m$$

$E' = E/(1-\upsilon)$, where E is Young's modulus, ν is Poisson's ratio, and V_m is the molar volume.

Considering the Gibbs free energy change, ΔG, accompanying the formation of a composition fluctuation, the condition for the coherent spinodal is

$$\frac{d^2 G}{dX^2} = -2\eta^2 E' V_m$$

The coherent spinodal line in the phase diagram is defined by this condition and is shown in Figure 4. It can be seen that the coherent spinodal is suppressed to a lower temperature by the coherency strain [20], meanwhile, a corresponding coherent miscibility gap is established, which defines the equilibrium compositions of the coherent phases that result from spinodal decomposition [19].

There are relatively few studies in the literature regarding the miscibility gap in ternary carbide systems. Kieffer et al. [6] experimentally established the miscibility gap in (Ti,Zr)C in equilibrium with Co. The critical temperature is reported to be 2100 °C. Markström and Frisk [21] evaluated the miscibility gap in the (Ti,Zr)C-Co system using both experimental and computational approaches and estimated the critical temperature to be 2050 °C. Li et al. [16] comprehensively investigated the phase diagram of (Ti,Zr)C, and suggested the top of the miscibility gap is between 2100 and 2200 °C.

As to (V,Nb)C, Kieffer et al. [6] experimentally investigated the miscibility gap of the system in equilibrium with Co, and the critical temperature of the miscibility gap was found to be around 1470 °C. Inoue et al. [22] found a similar result when investigating the phase diagram of (V,Nb)C system using an iron-based alloy. Frisk [23] estimated the miscibility gap using the Calphad (Calculation of Phase Diagram) method, considering the experimental result from Kieffer et al. [6] and Inoue et al. [22], and found the critical temperature of the miscibility gap to be 1600 °C with respect to the critical composition of $V_{0.6}Nb_{0.4}C$.

The miscibility gap of (V,Ta)C was also studied by Kieffer et al. [6], and according to their experimental results on (V,Ta)C with Co, the critical temperature is 1340 °C. Servant and Danon [24] estimated the miscibility gap in the (V,Ta)C system using the Calphad method and suggested the critical temperature as 1180 °C. Both studies estimated the critical composition is $V_{0.65}Nb_{0.35}C$.

2.3 Phase separation

(Ti,Zr)C

In earlier research, Knotek and Barimani [25] reported that decomposition occurs in magnetron-sputtered $Ti_{0.5}Zr_{0.5}C$ and $Ti_{0.3}Zr_{0.7}C$ films, where Ti-rich nano-region was observed to distribute on a Zr-rich matrix. In a composite sintered from a $Ti_{0.4}Zr_{0.4}W_{0.2}C$ powder with Co, Xu et al. [26] observed side bands in the X-ray diffraction pattern of the composite, and suggested that this was due to spinodal decomposition.

Recently, Borgh et al. [15] found that (Ti,Zr)C decomposes to a lamellar structure upon aging at 1300 °C. In the appended Paper I, it is verified that decomposition also occurs at 1400, 1600, and 1800 °C (Figure 5). The composition of as-decomposed phases was studied by EDS and XRD and is in good agreement with the calculated phase diagram (Figure 6). Upon aging at the same temperature, the composition of the lamellar structure estimated by XRD does not change over time and is thus unlikely to be spinodal decomposition. An EBSD study revealed that the adjacent lamellae share the same crystal orientation (see Papers I and III).

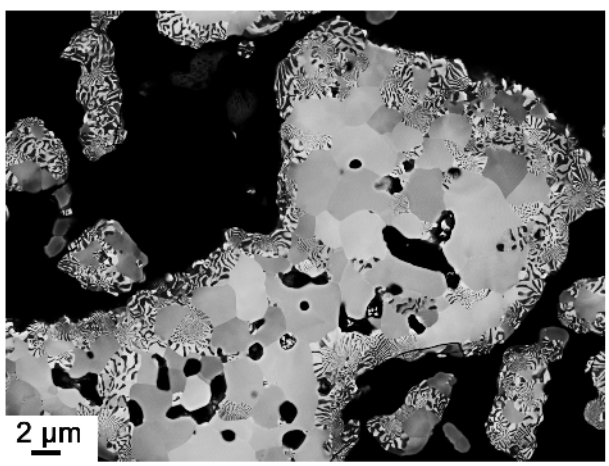

Figure 5. Decomposition in (Ti,Zr)C aged at 1800 °C for 20 h.

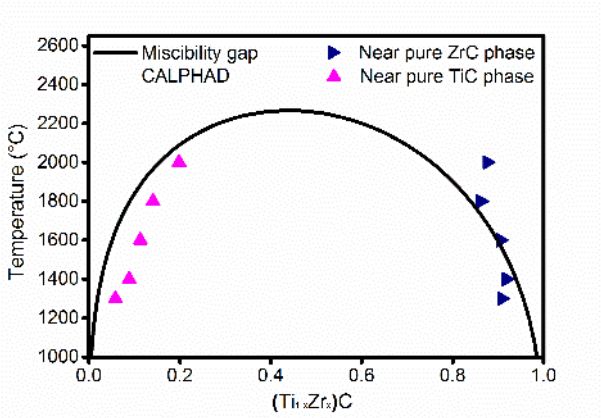

Figure 6. Miscibility gap in (Ti,Zr)C calculated using Calphad data and experimental data of the composition of decomposition.

Li. et al. [27] also reported that $Ti_{0.9}Zr_{0.1}C$ decomposed into a lamellar structure of $Ti_{0.97}Zr_{0.03}C$ and $Ti_{0.06}Zr_{0.94}C$ upon aging at 1300 °C. The orientation relation between the as-decomposed lamellae was found to be TiC-rich phase {100}// ZrC-rich phase {100} [16,27].

(V,Nb)C

In the appended Paper IV, it was found that the (V,Nb)C-Fe (0.5 wt % of Fe) decomposes into lamellae upon aging at both 900 and 1200 °C, and the decomposition mainly occurs around the sample edge. This kind of decomposition is very rare in (V,Nb)C aged in the same conditions. The small amount of Fe addition was, therefore, believed to facilitate the decomposition of (V,Nb)C.

(V,Ta)C

Different from the situation above, as-decomposed lamellar structure was found in the as-synthesized (V,Ta)C (see Paper IV). Upon aging at 1200 °C, more decomposition occurred, resulting in a larger amount of lamellae. However, a different type of microstructure—V-rich layers encircled by Ta-rich layers—formed in (V,Nb)C-Fe (0.5 wt % of Fe) upon aging at 1200 °C.

Hence, adding Fe seemed to affect the mechanism of phase separation in (V,Ta)C system.

2.4 Hardness

One of the most important properties of transition metal cubic carbides is their high hardness.

Holleck [5] reported (Ti,Hf)C to be super hard, around 43 GPa, and suggested this was due to hardening of the solid solution or phase separation within the miscibility gap.

Knotek and Barimani [25] found that the hardness of (Ti,Zr)C thin films decreases upon aging at 1000 °C and suggested that this was due to decomposition. In Paper III, nano-indentation hardness of (Ti,Zr)C powder was found to be 41±6 GPa, and the high hardness was maintained around the same level in a partially decomposed particle upon aging at 1300 °C for 500 h. In Paper II, fully decomposed (Ti,Zr)C grains were found to be 10% softer than unaged (Ti,Zr)C grains. Li et al. [16] showed that the hardness of (Ti,Zr)C can be improved by aging at different temperatures. The largest increase in hardness was around 10%.

According to Holleck [5], the Vicker hardness of (V,Nb)C solid solution is around 24 GPa, while as measured in Paper IV, the nano-indentation hardness of (V,Nb)C is 26.5±1 GPa, and the hardness is basically the same after the solid solution decomposed into a lamellar structure. Regarding (V,Ta)C, its Vicker hardness was reported to be around 28 GPa [5], and, comparably, its nano-indentation hardness was found to be 30.2±1.3 GPa (see Paper IV).

Chapter 3

Discontinuous precipitation

In the classical case of discontinuous precipitation, there are two reaction products: a solute-depleted matrix and a solute-rich precipitate with a different crystal structure compared to the matrix, usually arranged in a lamellar structure and growing behind a migrating former grain boundary [27] (see Figure 7). The solute-depleted matrix inherits the crystal orientation of the original matrix. In the case of discontinuous precipitation in a miscibility gap, this picture of the reaction is largely retained but there is a difference in that both lamellae have the same crystal structure and usually the same orientation as the grain behind the advancing grain boundary.

3.1 Discontinuous precipitation in miscibility gap

Cahn [20,29] suggested that the coherent spinodal may be suppressed by coherency strain and that discontinuous precipitation takes place instead to reduce the energy of the system. In the Au-Ni system at high temperature, due to high coherency strain, the decomposition is discontinuous precipitation; however, at low temperature, it is spinodal decomposition [20,30]. Other miscibility gap systems have also been found to decompose via discontinuous precipitation, e.g., W-Cr [31,32].

In Paper I and Paper III, it was found that (Ti,Zr)C decomposes through discontinuous precipitation at temperatures between 1300 °C to 1800 °C. In

Paper IV, (V,Nb)C and (V,Ta)C show discontinuous precipitation at 1200 °C (see Figure 8). In all the cases, it appears that the lamellae inherit the crystal orientation of the grain behind and grow with the migrating grain boundary.

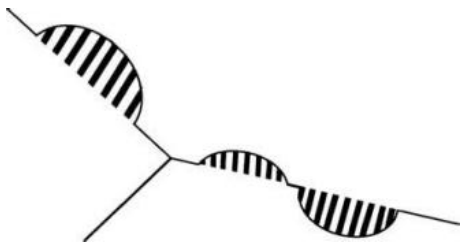

Figure 7. Schematic illustration of discontinuous precipitation [28].

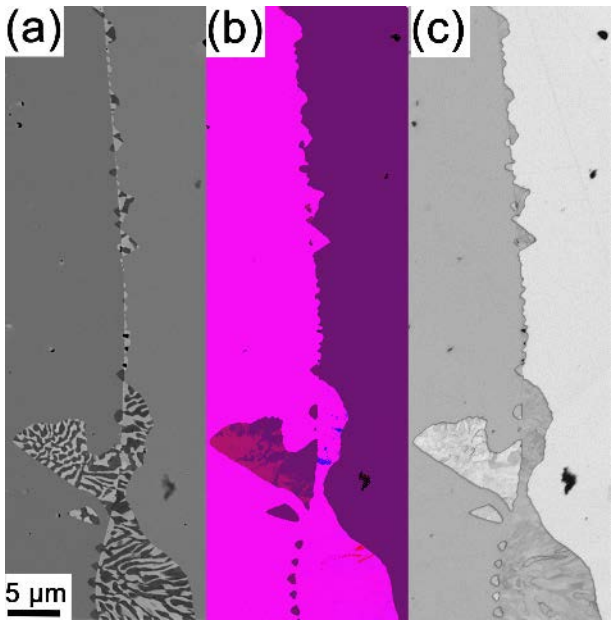

Figure 8. Discontinuous precipitation in (V,Nb)C: (a) SEM image with backscattered electrons, (b) and (c) Euler map and pattern quality of (a).

3.2 Initiation of discontinuous precipitation

Discontinuous precipitation has been found to occur at certain grain boundaries but is absent at others [33], and hence the reaction seems to be highly dependent on grain boundary properties. Since the grain boundary structure is highly dependent on grain boundary misorientation, a misorientation study was performed in the (Ti,Zr)C system (see Paper II). It was found that the decomposition occurs at high-angle grain boundaries, especially between 25 ° and 50 ° (see Figure 9). A similar phenomenon was revealed in an Al-Ag-Ga alloy [34], and it was suggested that it is the interfacial energy, connected with the grain boundary misorientation, which impacts the occurrence of DP. The difference in the interfacial energy of two long facets of the precipitate provides the driving force for the grain boundary migration as well as the progress of DP. Moreover, Monzen et al. [35,36] found that at boundaries with higher energy, the incubation period for the cell formation is shorter and cell growth rate is faster. In other words, the high-energy grain boundary facilitates both initiation and development of DP.

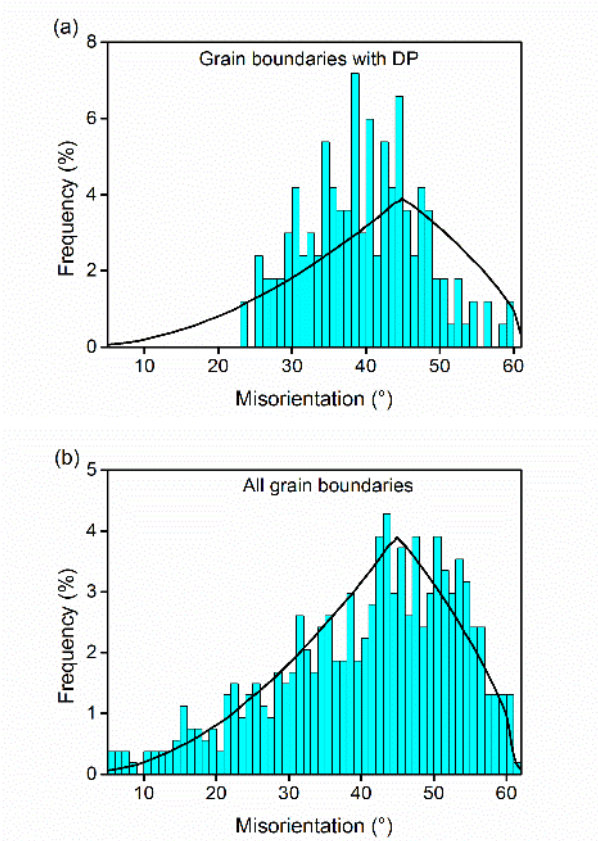

Figure 9. (a) Misorientation distribution of grain boundaries with discontinuous grain boundary precipitation, and (b) misorientation distribution of all grain boundaries.

Chapter 4

Sintering

Ternary cubic carbides may be sintered as a γ-phase with WC-Co to study the sintering behavior. The manufacturing process of cemented carbides includes milling, drying, compaction, dewaxing, and sintering. Firstly, the carbide powders and binder metal powder are milled with a compaction aid such as paraffin wax and polyethylene glycol (PEG). The milling is performed in alcohol or acetone using WC-Co rods as the milling body. Then, the slurry is spray dried and pressed into green compacts, which are then put into a furnace for dewaxing and sintering. Dewaxing is usually performed between 200 and 450 °C in hydrogen to remove the compaction aid. Then the furnace is evacuated to vacuum, and further heated to the sintering temperature, usually between 1400 and 1500 °C, which are over the melting point of the binder phase, and held for a while before cooling down (see Figure 10).

4.1 Microstructure evolution

The sintering process for cemented carbides can be divided into two stages: solid state and liquid state sintering.

Solid state sintering

It is well studied that a significant part of densification in cemented carbides occurs before binder melting [2,37]. According to Uhrenius et al. [38], oxides of W, Nb, Ta, and Ti can be reduced by carbon between 400 and 1150 °C. After the oxide layer being reduced, Co could diffuse out onto the carbide

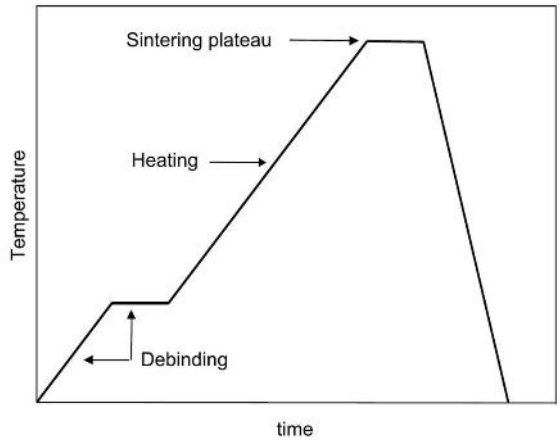

Figure 10. Sintering process of cemented carbides [37].

surfaces at rather low temperatures (< 1000 °C), meanwhile carbide particles start to agglomerate. Haglund et al. [39] reported that Co spreads on carbide phases from 1100 °C, and then it was suggested that the Co spreading on WC is associated with densification through the rearrangement of WC particles [40]. In other studies, Haglund et al. [41,42] also observed that sintering of WC-Co powder mixture begins around 800 °C, then simulated the dissolution behavior of WC in Co, and found that thinner binder regions reach equilibrium composition around 950 °C and in all regions of the sample, equilibrium is reached at 1200 °C.

For systems containing cubic carbonitrides, Zackrisson et al. [43] reported that an inner rim of (Ti,W)(C,N) forms onto undissolved Ti(C,N) powder particles during solid state sintering. Co binder acts as a transport medium for tungsten, titanium, carbon, and nitrogen elements to re-precipitate as inner and outer rims at solid and liquid phase sintering, respectively.

In Paper V, in WC-(Ti,Zr)C-Co cemented carbide, it was observed that (Ti,W,Zr)C γ_1-phase rims form around original (Ti,Zr)C particles during solid state sintering, and (Ti,Zr)C particles decompose into Ti-rich and Zr-rich lamellae at this stage (see Figure 13). The decomposition inside (Ti,Zr)C

particles is similar to the previously observed discontinuous precipitation in a ternary carbide system (see Paper I and II), but the kinetics is much faster, which could be attributed to the presence of Co and perhaps W.

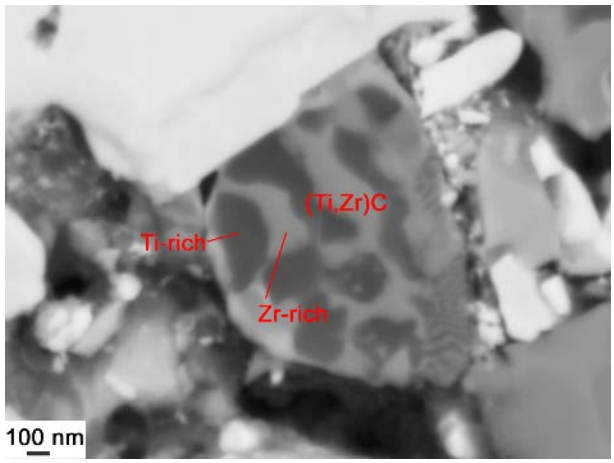

Figure 11. Decomposition in (Ti,Zr)C particles during solid state sintering.

Liquid state sintering

In this stage of sintering process, further dissolution and re-precipitation occur. Once the liquid is formed, its further formation and spread over particles are rapid, and during this period, densification occurs through rearrangement of particles, solution re-precipitation, and final coalescence. In the final stage of liquid phase densification, microstructural changes of practical importance – grain size, size distribution, grain shape, and binder phase distribution – take place, which significantly influence composite properties, such as wear resistance, strength, fracture toughness, magnetic properties, and ductility [2].

In the WC-(Ti,Zr)C-Co cemented carbide, (Zr,W,Ti)C γ_2-phase was observed to begin re-precipitation during liquid phase sintering (see Paper V), along with the further formation of (Ti,W,Zr)C γ_1-phase and decomposition of (Ti,Zr)C phase.

Final microstructure

In the WC-(Ti,Zr)C-Co composite, two γ-phases present in the final microstructure, which is in accordance with the calculated phase equilibrium using Thermo-Calc, and the phase compositions measured in the experiments and those from the calculation are in good agreement (see Paper V).

It is well known that the grain size of the carbide phase need to be carefully controlled, in order to achieve desired properties [3]. The hardness of the material depends to a large extent on WC grain size – generally, a smaller WC grain size means a harder material [44]. WC grain growth is seen due to Ostwald ripening, i.e. large grains growing at the expense of smaller ones, while the addition of VC, TiC, NbC, ZrC, and TaC can effectively inhibit WC grain growth during sintering [44,45].

In Paper V, with the addition of equal amounts of Ti and Zr in WC-(Ti,Zr)C-Co, the average grain size of both WC and two γ-phase particles is 10% smaller than those in WC-TiC-ZrC-Co.

In WC-(Ti,Zr)C-Co, undissolved Zr-rich (Ti,Zr)C is found in γ_2-grains as dark cores (see Figure 12); however, the γ_2-grains in WC-TiC-ZrC-Co composite are homogeneous, i.e., free from a dark core. During the sintering process, there is competition between dissolution of both the Ti-rich and Zr-rich (Ti,Zr)C phases in WC-(Ti,Zr)C-Co, and it is believed that the dissolution of Zr-rich phase is refrained and retained in the final microstructure.

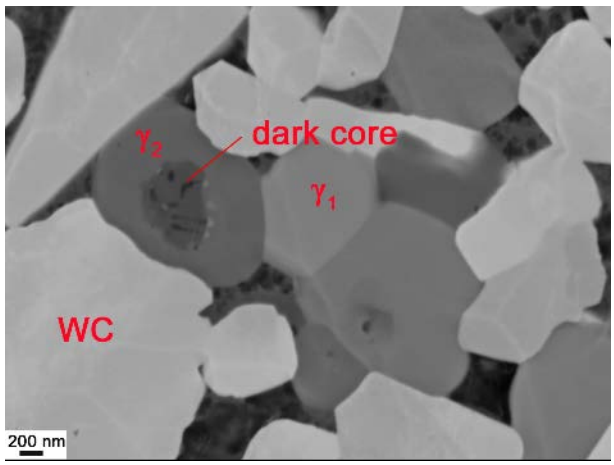

Figure 12. Dark core in WC-(Ti,Zr)C-Co composite.

4.2 Mechanical properties

Cemented carbides find applications largely due to their high wear resistance. In practice, hardness tests are often used as an indication for the wear performance, since it is known that hardness affects wear rate. Hardness is dependent on cobalt content, average grain size, and the composition of hard grains. The addition of cubic carbides, e.g., TaC and TiC, increases the resistance of WC-Co composites to plastic deformation and reduces the rate of strength loss with increasing temperature. It is believed that the contribution to increased hot hardness is due to the appreciably higher hardness of their complex solid solution, e.g., (W,Ti)C, (W,Ta)C, (W,Ti,Ta)C as compared to their individual solid solutions [2].

Weidow et al. [44] showed that addition of both TiC and ZrC into WC-Co cemented carbides can more effectively inhibit grain growth, compared to adding only TiC or ZrC, and lead to higher hardness. Xu et al. [26] investigated sintering using single phase (W,Ti,Zr)C powder with Co powder and found that composites with starting material of $(W_{0.2}Ti_{0.4}Zr_{0.4})C$ decomposed spinodally, and the resulting composite is 20 % harder. Hall and Retelsdorf [46] sintered (Ti,Zr)C with WC-Co and reported to have produced spinodal decomposition structures in the fine-grained composite,

which also showed high resistance to abrasion. In Paper V, both WC-(Ti,Zr)C-Co and WC-TiC-ZrC-Co composites showed a similar hardness although the carbide grain size in the former composite was 10% smaller.

Chapter 5

Characterization of carbides

5.1 Scanning electron microscopy (SEM)

SEM is commonly used to characterize the microstructure of a wide range of materials. The electron beam generated from an electron gun interacts with a specimen in a vacuum, producing many types of signals (see Figure 13), which can be transformed to images through corresponding detectors. Field emission SEM has high resolution to below 1 nm for imaging. Depth-of-field is another advantage of SEM as compared to light microscopy.

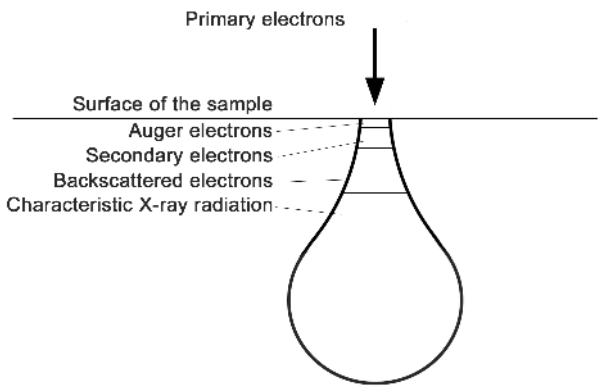

Figure 13. Schematic illustration of electron-specimen interaction.

Secondary electron micrographs are generated by collecting secondary electrons, which are outer shell electrons ejected from specimen atoms during inelastic scattering of the incident electron beam. The signal comes from a shallow depth beneath the surface of about 5-50 nm, and is therefore commonly used to reveal surface topography.

On the other hand, backscattered electron micrographs are generated by collecting backscattered electrons, which are generated when the incident electron beam interacts with nucleus and the electrons of atoms in the specimen, and is backscattered. The incident electron beam largely changes direction and escapes the specimen, and the resulting signal can reveal not only atomic number contrast but also crystal orientation contrast. Constituents in the microstructure with a higher atomic number produce more backscattered electrons and appear as brighter features in the image. This method is very useful for studies of phase separation in ternary carbides and microstructure of cemented carbide.

5.2 Energy dispersive spectroscopy (EDS)

SEM can be equipped with EDS, using characteristic X-rays to determine the composition both qualitatively and quantitatively. Characteristic X-rays are X-ray photons generated when outer shell electrons fill the inner-shell vacancies, which are sharply defined energy transitions and characteristic to each element. This method can be mainly applied to analyze elements with larger atomic numbers.

X-ray spatial resolution is the maximum width and depth of the electron interaction volume, usually in the order of 1 μm, depending on the incident electron beam energy (conventionally 10-30 keV) and critical excitation energy.

Low-voltage microanalysis (<= 5 keV) results in smaller interaction volumes and thus higher resolution. Monte Carlo electron trajectory simulation [47,48] is shown in Figure 14 to exemplify the smaller interaction volume at 5 kV as

compared to 10 kV applied acceleration voltage. The EDS line scan through (Ti,Zr)C lamellae in Figure 15 was performed in low-voltage mode.

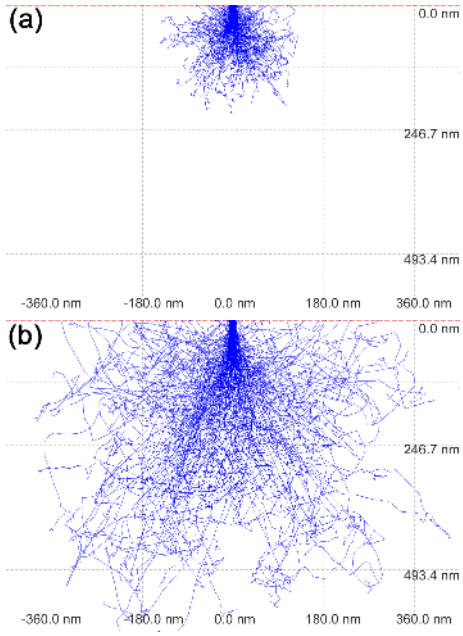

Figure 14. Monte Carlo simulation of electron trajectory in (Ti,Zr)C sample under the beam energy of (a) 5 kV and (b) 10 kV.

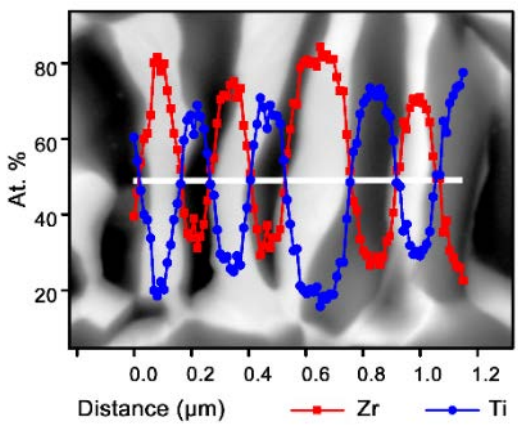

Figure 15. EDS line scan through (Ti,Zr)C nano-scale lamellae at low beam energy.

Another useful function is the compositional map. EDS mapping was used to analyze sintered samples with multiple elements.

5.3 Electron backscatter diffraction (EBSD)

SEM can also be equipped with EBSD, which can be applied to study crystallography, e.g., crystal structure and grain orientation. The measurement is usually performed by tilting a sample to a high degree, usually 70° from the horizontal position, and illuminating it by the electron beam. Kikuchi diffraction forms flat cones intercepting the image plane, i.e., a camera, generating the backscattered Kikuchi diffraction patterns (see Figure 16).

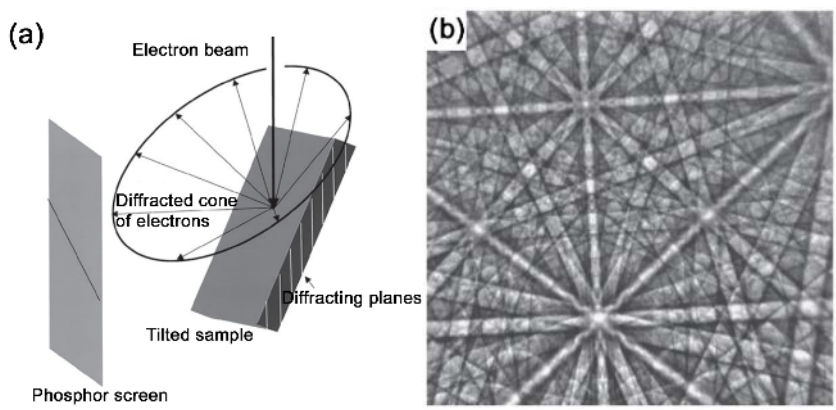

Figure 16. (a) Schematic illustration of the arrangement of the sample and the phosphor screen, and (b) an example of Kikuchi patterns [49].

EBSD maps can be produced through automated indexing of Kikuchi patterns and computer-automated crystal lattice orientation mapping. The Euler map is based on the crystallographic orientation in Euler space, and the corresponding orientation is represented by a set of Euler angles. Pattern quality is the quantity expressed based on the extent of blurring of Kikuchi patterns, which indicates the density of point defects, dislocations, or lattice strain. For example, the grain boundaries are identified as low pattern quality, i.e., a dark colour.

Misorientation represents the difference in the orientation between grains or other features. The misorientation angle is the difference in angle between two grains and can be described by angle/axis pairs, with the angle rotated around a common axis [50].

5.4 X-ray diffraction (XRD)

When an X-ray beam strikes and is scattered by an atom, the atom scatters radiation in different directions. For crystalline materials, the atoms are periodically arranged, and then the scattered radiation could undergo diffraction. The condition for constructive interference can be described by Bragg's law (see Figure 17),

$$\lambda = 2d\ sin\theta$$

where λ is the wavelength of the incident X-rays, 2θ is the angle between the incident and the diffracted X-ray beam, and d is interplanar spacing. In a cubic crystal with lattice parameter a, there is the following relation

$$d = \frac{a}{\sqrt{h^2+k^2+l^2}}$$

where h, k, and l are Miller indices of the crystal plane.

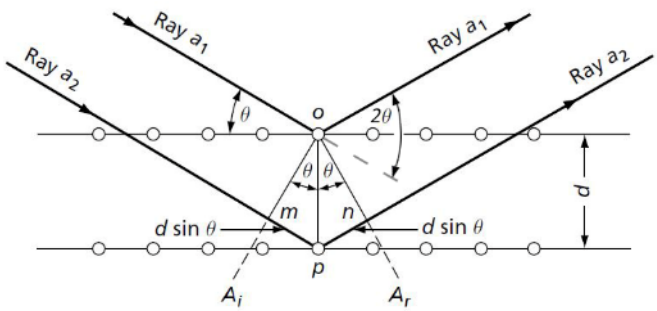

Figure 17. Bragg's law [51].

When a monochromatic X-ray beam strikes a specific crystal, constructive interference could only occur at several strictly defined diffraction angles, which is then represented by diffraction peaks against 2θ in XRD patterns.

For a continuous solid solution, A_xB_{1-x}, there is a linear relationship between the lattice parameter and composition,

$$a_{A_{(1-x)}B_x} = (1-x)a_A + xa_B$$

which is known as Vegard's law.

In such cases, XRD can be used to determine the composition of phases. First, the diffraction angle can be calculated using Gaussian fitting (Figure 18). Thereafter, the lattice parameter and composition can be determined consecutively.

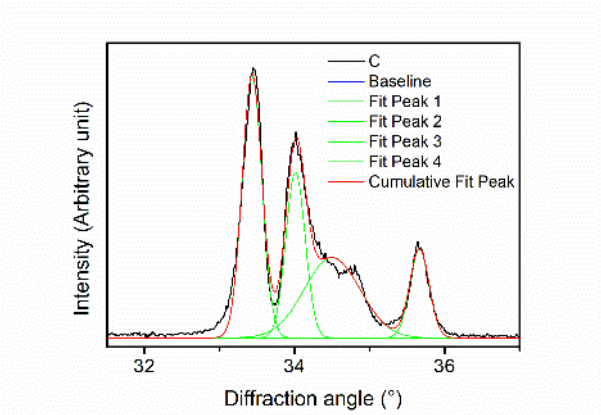

Figure 18. Example of a Gaussian fitting of XRD pattern of (Ti,Zr)C aged at 1400 °C for 100 h.

5.5 Nano-indentation

Nano-indentation, usually with a Berkovich indenter, is a primary technique for determining local hardness of small structural features and thin film specimens. Except the scale of indents, another significant difference of nano-indentation from traditional hardness measurement is the load- and depth-

sensing feature – the load and depth is recorded during each indentation process. An example of load and depth compliance is shown in Figure 19.

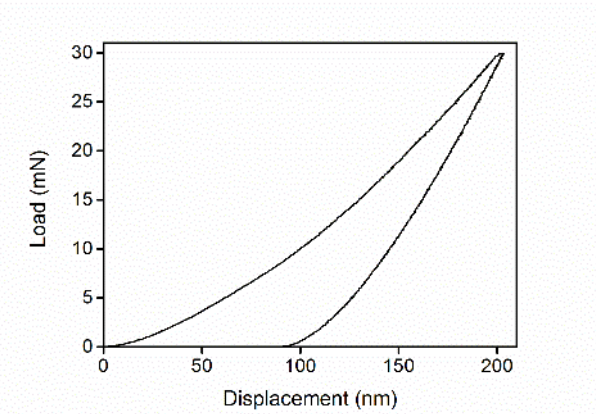

Figure 19. Load-displacement curve recorded during an indentation measurement on (V,Nb)C

Nano-indentation hardness is defined as

$$H = \frac{P_{max}}{A}$$

where P_{max} is peak load, and A is contact area.

P_{max} is well recorded during measurement, but A is more difficult to define and it is an important factor affecting the accuracy of hardness measurements.

There are two classes of methods to determine the contact area: indirect calculation, e.g., Oliver and Pharr's method [52], and direct imaging. The indirect calculation is time-saving but highly dependent on the accuracy of the area function, which is defined by the geometry of the indenter and the contact height and needs to be carefully calibrated according to range of indentation depth. However, it has been found that when the indentation depth is shallower than 200 nm, large errors can occur due to the imperfect shape of indenter tips [53].

Direct imaging is usually performed using SEM [52,53] (see Figure 20) or a topography imaging microscopy, e.g., scanning probe microscopy (SPM)[54]. The advantage of this method is that the area measurement is insensitive to the stiffness of the sample holder and indentation machine, which is particularly important for small samples and hard materials, e.g., carbides. For materials with significant pile-up phenomenon, the direct imaging method is also more accurate. Furthermore, the direct method can be applied to both deep and shallow indentations.

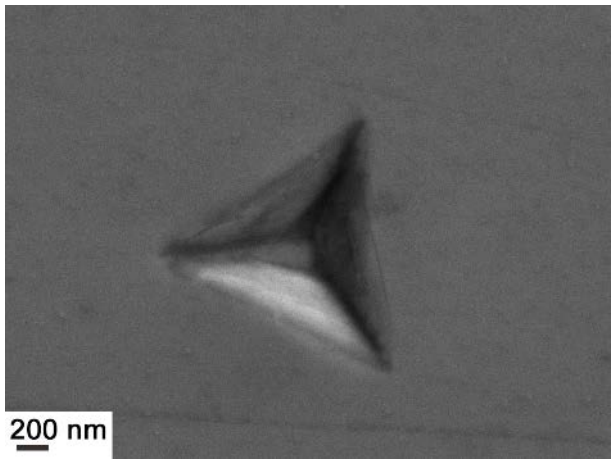

Figure 20. SEM micrograph using secondary electrons of an indent in (V,Nb)C

Chapter 6

Summary of appended papers

Paper I Microstructure evolution during phase separation in Ti-Zr-C

(Ti,Zr)C powder was synthesized by carbothermal reduction and subsequently aged at 1150–2000 °C. It was found that the as-synthesized (Ti,Zr)C particles have a concentration gradient with a higher concentration of Ti at the surface of the particles. Furthermore, during aging, the (Ti,Zr)C decomposes into Ti-rich and Zr-rich lamellae. During aging at 1400 and 1800 °C for 10 h, most of the Zr-rich and Ti-rich domains precipitate at grain boundaries, inheriting the crystal orientation of the parent grain behind the growth front. When the precipitate grows into another (Ti,Zr)C grain, that grain adopts the same crystal orientation as the parent grain. Based on these microstructural observations, it is hypothesized that the mechanism of decomposition is discontinuous precipitation.

Paper II Synthesis, aging and nano-hardness of Ti-Zr-C

(Ti,Zr)C micro-sized powder was synthesized through carbothermal reductions at 2200 °C, 2300 °C, and 2400 °C. The as-synthesized carbides were thereafter aged at 1400 °C to study phase separation. The effect of synthesis temperature on the composition and morphology of as-synthesized

carbides was investigated. An analysis of the distribution of grain boundary misorientations was performed to investigate the dependence of discontinuous precipitation on misorientation. A nano-indentation study was performed on both fully decomposed particles and unaged particles. The effect of Co on phase separation was also investigated.

Paper III Self-organizing nanostructured lamellar (Ti,Zr)C – A superhard mixed carbide

A nano-indentation and first-principles calculation study of a self-organizing nanostructured lamellar (Ti,Zr)C was performed. Nano-indentation measurements revealed that the hardness of carbide is comparable to the hardest transition metal carbides that have been previously reported. The origin of the super-high hardness is postulated to be the inherent bond strength and large coherency strains that are generated when the carbide demixes within the miscibility gap. The high hardness is maintained at a high level even after 500 h aging treatment at 1300 °C. Therefore, it is believed that the new superhard mixed carbide has high potential in various engineering applications such as in bulk cemented carbide and cermet cutting tools and in surface coatings.

Paper IV Powder-metallurgical synthesis and aging of (V,Nb)C and (V,Ta)C

The ternary carbides (V,Nb)C and (V,Ta)C were synthesized by heating powder mixtures of the corresponding binary carbides. Different mixing conditions were utilized to study the effect of mixing on synthesis. The homogeneity of (V,Nb)C and (V,Ta)C was improved by adding small amounts of Fe powder, followed by milling. The as-synthesized carbides were aged at 900 °C and 1200 °C, which are inside the miscibility gap for each system, to study decomposition.

It was found that (V,Nb)C, with small additions of Fe, decomposed in a way that resembles discontinuous precipitation upon aging at 1200 °C. (V,Ta)C with and without additions of Fe were found to decompose upon aging at

1200 °C, but had a different morphology compared to (V,Nb)C. The hardness of both as-synthesized and aged carbides was measured using nano-indentation and was found to be 26.5±1 GPa and 30.2±1.3 GPa for (V,Nb)C and (V,Ta)C, respectively. High hardness was found to be maintained in (V,Nb)C after decomposing into V-rich and Nb-rich lamellae.

Paper V Liquid phase sintering of (Ti,Zr)C with WC-Co

(Ti,Zr)C powder was sintered with WC-Co following an industrial process, including an isotherm at 1410 °C. A series of interrupted sintering trials was performed with the aim of studying the sintering behavior and the microstructural evolution during both solid state and liquid state sintering. Reference samples, using the same elemental compositions but with the starting components TiC and ZrC instead of (Ti,Zr)C, were also sintered.

It was found that the (Ti,Zr)C phase decomposes into Ti-rich and Zr-rich nano-scale lamellae before the liquid state of the sintering initiates. The final microstructure consists of the binder and WC as well as two different phases, rich in either Ti (γ_1) or Zr (γ_2). The γ_2 phase grains have a core-shell structure with a (Ti,Zr)C core following the full sintering cycle. The major differences observed in (Ti,Zr)C with respect to the reference samples after the full sintering cycle were the referred core-shell structure and the carbide grain sizes; additionally, the microstructural evolution during sintering differs. The grain size of carbides (WC, γ_1, and γ_2) is about 10% smaller in WC-(Ti,Zr)C-Co than in WC-TiC-ZrC-Co. The shrinkage behavior and hardness of both composites are reported and discussed.

Chapter 7

Concluding remarks and future work

In this thesis, (Ti,Zr)C, (V,Nb)C, and (V,Ta)C ternary cubic carbides were synthesized using traditional powder-metallurgical methods. It was found that the synthesis temperature affects both compositional and morphological homogeneity of (Ti,Zr)C powder particles formed through the carbothermal reduction, and the homogeneity improved as the synthesis temperature increased. Other factors, such as mixing condition and diffusion aids, were also found to affect the homogeneity of as-synthesized (V,Nb)C and (V,Ta)C. Those synthesized from binary carbide powders milled with small amount of Fe (0.5 wt%) showed significantly lower porosity.

Upon aging between 1150-1800 °C, (Ti,Zr)C decomposed to Ti-rich and Zr-rich lamellae, which were found to initiate at grain boundaries, inherit the crystal orientation of the grain behind, and advance toward an adjacent grain with a migrating grain boundary. This corresponds to the characteristics of discontinuous precipitation.

With regard to (V,Nb)C, after aging at 1200 °C for 500 h, the alloy with addition of Fe decomposed to lamellae. Most decomposition occurred on the sample edges, while those at the interior of the sample were found to be discontinuous precipitation. However, little decomposition occurred in the

alloy without diffusion aid aged at the same condition. It is therefore believed that the decomposition of (V,Nb)C was enhanced by small amount of Fe.

The role of Fe in (V,Ta)C was however different from above. Without Fe, there was already a few decomposition along grain boundaries in as-synthesized (V,Ta)C, which were found to be discontinuous precipitation. More decomposition occurred in the alloy upon aging at 1200 °C for 500 h. In comparison, the alloy with addition of Fe was free from decomposition after synthesis, and then slightly decomposed upon aging at 1200 °C for 500 h, but forming a different morphology than lamellae. It seems the addition of Fe not only inhibited the rate of decomposition but also affected the mechanism of the decomposition in (V,Ta)C.

Using the nano-indentation technique, the hardness of both carbide particles and decomposed structures were investigated. The hardness of as-synthesized (Ti,Zr)C particles were found to be 41 ± 6 GPa, and the decomposed particles are slightly softer, with a hardness of 34 ± 3 GPa. Both as-synthesized (V,Nb)C and decomposed grains were found to have a hardness around 26 GPa. It shows the discontinuous precipitation has limited influence on the hardness of ternary carbides.

Furthermore, when (Ti,Zr)C particles were sintered with WC-Co, significant decomposition of (Ti,Zr)C occurred already during solid state sintering. The final microstructure contained two γ-phases, rich in either Ti (γ_1) or Zr (γ_2). The latter had a core-shell structure with a core of undissolved Zr-rich (Ti,Zr)C phase, whose dissolution is supposed to be inhibited by the Ti-rich counterpart. The grain size of carbides (WC, γ_1, and γ_2) was about 10% smaller in WC-(Ti,Zr)C-Co than in WC-TiC-ZrC-Co.

Although some aspects of microstructure evolution during aging of different ternary carbides have been studied in the present work, there are, however, still many challenging aspects that need further investigation:

- The coherency condition of the as-decomposed lamellae of (Ti,Zr)C, (V,Nb)C, and (V,Ta)C is not understood. The preferred orientation

relationship between decomposed phase and the matrix, towards which the grain boundary advances, is unknown. It is important to understand this condition for decomposition.

- The effect of coherency strain on decomposition needs further investigation. Meanwhile, it is also unclear how defects, e.g., free surface and concentration inhomogeneity, affect decomposition.
- The effect of lamellar spacing on hardness is worth studying to better understand the properties of ternary carbides.
- The decomposition at low temperatures in all carbide systems is unknown. Spinodal decomposition may occur at low temperatures.
- The addition of Fe in (V,Nb)C was found to significantly enhance the decomposition, but the role of Fe is not well understood.
- The addition of Fe in (V,Ta)C resulted in different decomposition mechanism, which is also not understood.
- (Ti,Zr)C particles in WC-(Ti,Zr)C-Co composite decomposed during the early sintering stage and finally formed two different γ-phase grains. To utilize the high hardness of ternary cubic carbides, some moderation needs to be made either in the sintering process, such as preforming solid state sintering, or the starting composition, e.g., using carbide powders with composition close to the final equilibrium composition and/or low binder content.

Acknowledgements

In the past 4.5 years, I had a very special journey as a PhD student at KTH. This was a time full of wondering and challenges.

I am very grateful to my supervisor Joakim Odqvist for giving me the opportunity to start this journey and also for his support through the whole study. I am also grateful to my co-supervisor Peter Hedström for his instruction on experiments and inspiring discussions. Their careful guidance lead me to the end of my PhD study, and their broad-mindedness encouraged me to explore research freely.

During my study, I received plenty of help from many people. I really appreciate the instruction from Ida Borgh at the beginning of my PhD study. I would also like to thank Rafael Borrajo-Pelaez for his help with microscopy measurement and analysis, which was a precious opportunity for me to learn experimental design and data analysis. Susanne Norgren and Andreas Blomqvist are thanked for their many helpful discussions. Valter Ström is thanked for help with nano-indentation study. Bjoern Glaser is thanked for help with high temperature heat treatment. Mari-Louise Englund is thanked for help with dilatometer and differential scanning calorimeter measurements. Emi Kiritani is acknowledged for the synthesis of ternary carbides. I also appreciate the nice working environment created by all my colleagues.

I acknowledge the support from VINN Excellence Center Hero-m. I truly appreciate the financial support from the Chinese Scholarship Council (CSC), Stiftelsen Axel Hultgren Fond, Bergshögskolans Jubileumsfond, and the Foundation for Applied Thermodynamics (STT).

Finally, I would like to thank Yuxuan Sun (孙宇轩) for support in all aspects. I am also thankful to my parents and parents-in-law for their understanding and encouragement.

Bibliography

1. Ortner, H. M.; Ettmayer, P.; Kolaska, H. The history of the technological progress of hardmetals. *Int. J. Refract. Met. Hard Mater.* **2014**, *44*, 148–159.

2. Upadhyaya, G. S. *Cemented Tungsten Carbides*; Elsevier, 1998.

3. Prakash, L. Fundamentals and general applications of hardmetals. In *Comprehensive Hard Materials*; Elsevier, 2014; pp. 29–90.

4. Pandemo, U. *Inorg. Mater.* **1967**, 1170. (As referenced in Holleck H. Metall. **1981**, 35, 999.)

5. Holleck, H. Material selection for hard coatings. *J. Vac. Sci. Technol. A Vacuum, Surfaces, Film.* **1986**, *4*, 2661.

6. Kieffer, R.; Nowotny, H.; Neckel, A.; Ettmayer, P.; Usner, L. Zur entmischung von kubischen mehrstoffcarbiden. *Monatshefte für Chemie* **1968**, *99*, 1020–1027.

7. Hörling, A.; Hultman, L.; Odén, M.; Sjölén, J.; Karlsson, L. Mechanical properties and machining performance of Ti1−xAlxN-coated cutting tools. *Surf. Coatings Technol.* **2005**, *191*, 384–392.

8. Mayrhofer, P. H.; Hörling, A.; Karlsson, L.; Sjölén, J.; Larsson, T.; Mitterer, C.; Hultman, L. Self-organized nanostructures in the Ti–Al–N system. *Appl. Phys. Lett.* **2003**, *83*, 2049.

9. Mayrhofer, P. H.; Mitterer, C.; Clemens, H. Self-organized nanostructures in hard ceramic coatings. *Adv. Eng. Mater.* **2005**, *7*, 1071–1082.

10. Toth, L. E. *Transition Metal Carbides and Nitrides*; Refractory materials;

Academic Press, 1971.

11. Schwarzkopf, P.; Kieffer, R. *Refractory Hard Metals: Borides, Carbides, Nitrides, and Silicides*; Macmillan, 1953.

12. Teber, A.; Schoenstein, F.; Têtard, F.; Abdellaoui, M.; Jouini, N. The effect of Ti substitution by Zr on the microstructure and mechanical properties of the cermet Ti1-xZrxC sintered by SPS. *Int. J. Refract. Met. Hard Mater.* **2012**, *31*, 132–137.

13. Liu, S.; Hu, W.; Xiang, J.; Wen, F.; Xu, B.; Yu, D.; He, J.; Tian, Y.; Liu, Z. Mechanical properties of nanocrystalline TiC–ZrC solid solutions fabricated by spark plasma sintering. *Ceram. Int.* **2014**, *40*, 10517–10522.

14. Lee, G.-G.; Ha, G.-H. Synthesis of ultra fine titanium-tungsten carbide powder from titanium dioxide and ammonium metatungstate. *Mater. Trans.* **2009**, *50*, 187–191.

15. Borgh, I.; Hedström, P.; Blomqvist, A.; Ågren, J.; Odqvist, J. Synthesis and phase separation of (Ti,Zr)C. *Acta Mater.* **2014**, *66*, 209–218.

16. Li, Y.; Katsui, H.; Goto, T. Effect of heat treatment on the decomposition of TiC–ZrC solid solutions by spark plasma sintering. *J. Eur. Ceram. Soc.* **2016**.

17. Norton, J. T.; Mowry, A. Solubility relationships of the refractory monocarbides. *Trans. Am. Inst. Min. Metall. Eng.* **1949**, *185*, 133–136.

18. Holleck, H. Ternäre carbidsysteme der hochschmelzenden übergangsmetalle- teil I. *Met. und Tech.* **1981**, *35*, 999–1004.

19. Porter, D. A.; Easterling, K. E.; Sherif, M. *Phase Transformations in Metals and Alloys, Third Edition*; CRC Press, 2009.

20. Cahn, J. W. On spinodal decomposition. *Acta Metall.* **1961**, *9*, 795–801.

21. Markström, A.; Frisk, K. Experimental and thermodynamic evaluation of the miscibility gaps in MC carbides for the C–Co–Ti–V–W–Zr system. *Calphad* **2009**, *33*, 530–538.

22. Inoue, K.; Ishikawa, N.; Ohnuma, I.; Ohtani, H.; Ishida, K. Calculation

of phaseequilibria between austenite and (Nb, Ti, V)(C, N) in microalloyed steels. *ISIJ Int.* **2001**, *41*, 175–182.

23. Frisk, K. Thermodynamic modelling of multicomponent cubic Nb, Ti and V carbides/carbonitrides. *Calphad* **2008**, *32*, 326–337.

24. Servant, C.; Danon, C. A. CALPHAD modelling of the unmixing of transition metal carbide phases. *Calphad* **2004**, *28*, 337–353.

25. Knotek, O.; Barimani, A. On spinodal decomposition in magnetron-sputtered (Ti,Zr) nitride and carbide thin films. *Thin Solid Films* **1989**, *174*, 51–56.

26. Xu R, Huang P, Y. H. Investigation on spinodal decomposition of WC-TiC-ZrC-Co cemented carbide. In *International powder metallurgy conference, Orlando, FL*; 1988; pp. 15–21.

27. Li, Y.; Katsui, H.; Goto, T. Phase decomposition of TiC–ZrC solid solution prepared by spark plasma sintering. *Ceram. Int.* **2015**, *41*, 14258–14262.

28. Aaronson, H. I.; Enomoto, M.; Lee, J. K. *Mechanisms of Diffusional Phase Transformations in Metals and Alloys*; 2010.

29. Cahn, J. The kinetics of cellular segregation reactions. *Acta Metall.* **1959**, *7*, 18–28.

30. Zhao, J.-C.; Notis, M. R. Ordering transformation and spinodal decomposition in Au-Ni alloys. *Metall. Mater. Trans. A* **1999**, *30*, 707–716.

31. Porter, D. E. The decomposition of tungsten-chromium solid solution. *Acta Metall.* **1967**, *15*, 721–726.

32. Den Broeder, F. J. A.; Burgers, W. G. An x-ray diffraction study of the decomposition of tungsten-chromium solid solution. *Acta Metall.* **1968**, *16*, 265–268.

33. Williams, D. B.; Butler, E. P. Grain boundary discontinuous precipitation reactions. *Int. Mater. Rev.* 1981, *26*, 153–183.

34. Hirth, S.; Gottstein, G. Misorientation effects on discontinuous

precipitation in Al–Ag–Ga. *Acta Mater.* **1998**, *46*, 3975–3984.

35. Monzen, R.; Shigehara, H.; Kita, K. Misorientation dependence of discontinuous precipitation in Cu-Be alloy bicrystals. *J. Mater. Sci.* **2000**, *35*, 5839–5843.

36. Monzen, R.; Watanabe, C.; Mino, D.; Saida, S. Initiation and growth of the discontinuous precipitation reaction at [011] symmetric tilt boundaries in Cu–Be alloy bicrystals. *Acta Mater.* **2005**, *53*, 1253–1261.

37. Allibert, C. H. Sintering features of cemented carbides WC–Co processed from fine powders. *Int. J. Refract. Met. Hard Mater.* **2001**, *19*, 53–61.

38. Uhrenius, B.; Agren, J.; Haglund, S. On the sintering of cemented carbides. In *Sintering Technology*; German, R.; Messing, G.; Cornwall, R., Eds.; Marcel Dekker: New York, 1996; pp. 129–139.

39. Haglund, S.; Ågren, J.; Uhrenius, B. Solid state sintering of cemented carbides : An experimental study. *Zeitschrift für Met.* **1998**, *89*, 316–322.

40. Missiaen, J.-M.; Roure, S. A general morphological approach of sintering kinetics: application to WC–Co solid phase sintering. *Acta Mater.* **1998**, *46*, 3985–3993.

41. Haglund, S.; Ågren, J.; Lindskog, P.; Uhrenius, B. Solid state sintering of cemented carbides. In *Sintering Technology*; German, R.; Messing, G.; Cornwall, R., Eds.; Marcel Dekker: New York, 1996; pp. 141–148.

42. Haglund, S.; Ågren, J. W content in Co binder during sintering of WC–Co. *Acta Mater.* **1998**, *46*, 2801–2807.

43. Zackrisson, J.; Andrén, H.-O.; Rolander, U. Development of cermet microstructures during sintering. *Metall. Mater. Trans. A* **2001**, *32*, 85–94.

44. Weidow, J.; Zackrisson, J.; Jansson, B.; Andrén, H.-O. Characterisation of WC-Co with cubic carbide additions. *Int. J. Refract. Met. Hard Mater.* **2009**, *27*, 244–248.

45. Hayashi, K.; Fuke, Y.; Suzuki, H. Effects of addition carbides on the grain size of WC-Co alloy. *J. Japan Soc. Powder Powder Metall.* **1972**, *19*, 67–71.

46. Hall, F. W.; Retelsdorf, H. J. Sintered hardmetals 1984.

47. Drouin, D.; Hovington, P.; Gauvin, R. CASINO: A new Monte Carlo code in C language for electron beam interactions-part II: Tabulated values of the mott cross section. *Scanning* **2006**, *19*, 20–28.

48. Hovington, P.; Drouin, D.; Gauvin, R. CASINO: A new Monte Carlo code in C language for electron beam interaction -part I: Description of the program. *Scanning* **2006**, *19*, 1–14.

49. Goldstein, J. I.; Newbury, D. E.; Echlin, P.; Joy, D. C.; Lyman, C. E.; Lifshin, E.; Sawyer, L.; Michael, J. R. *Scanning Electron Microscopy and X-ray Microanalysis*; Springer US: Boston, MA, 2003.

50. Schwartz, A. J.; Kumar, M.; Adams, B. L.; Field, D. P. *Electron Backscatter Diffraction in Materials Science*; Springer US: Boston, MA, 2009.

51. Abbaschian, R.; Abbaschian, L.; Reed-Hill, R. E. *Physical Metallurgy Principles*; Edition, 4, Ed.; CL Engineering, 2008.

52. Oliver, W. C.; Pharr, G. M. An improved technique for determining hardness and elastic modulus using load and displacement sensing indentation experiments. *J. Mater. Res.* **1992**, *7*, 1564–1583.

53. Oliver, W. C.; Pharr, G. M. Measurement of hardness and elastic modulus by instrumented indentation: Advances in understanding and refinements to methodology. *J. Mater. Res.* **2004**, *19*, 3–20.

54. Charleux, L.; Keryvin, V.; Nivard, M.; Guin, J.-P.; Sanglebœuf, J.-C.; Yokoyama, Y. A method for measuring the contact area in instrumented indentation testing by tip scanning probe microscopy imaging. *Acta Mater.* **2014**, *70*, 249–258.